Compact high-gain volumetric phased array antenna with genetically designed inter-element resonances for 5G applications

V.D. Burtsev[1,*], T.S. Vosheva[1], N.O. Bulatov[1], A.A. Khudykin[2], P. Ginzburg[3] & D.S. Filonov[1]

[1]Center for Photonics and 2D Materials, MIPT, Dolgoprudny 141701, Russia
[2]Telecom R&D Center, MIPT, Dolgoprudny 141701, Russia
[3]School of Electrical Engineering, Tel Aviv University, Tel Aviv 69978, Israel

Abstract:

High-gain directive antennas are used to support point-to-point long-range wireless communication channels. In typical designs, the array factor plays the key role, while individual elements layout is simplified. Here we demonstrate a 4-elements phased array, where a volumetric form factor of each element is taken as an advantage to elevate the antenna gain while keeping the device footprint small. The two-step design process, encompassing a genetic topology optimization and finite tuning with a particle swarm algorithm, is applied and subsequently demonstrated. We show that exploring the third dimension allows obtaining more than 25dB isolation between adjacent radiating elements and, at the same time, grants them highly directive radiation patterns. This operation principle is verified by demonstrating a large number of resonating multipoles constructively interfering to create a directional beam. The antenna with a $\pi\lambda^2$ aperture demonstrated more than 13 dB gain around 3GHz frequency range. Antenna elements were 3D-printed in resin and then metalized electrochemically. Additive manufacturing of complex volumetric architectures with a small inter-element spacing allows implementing new devices, encompassing the advantages of resonant approaches and arrays factors. Miniaturized 3D antenna array devices can find a use in wireless communications, where controllable beam properties, including high gain, are demanded.

*corresponding author: burtsev.vd@phystech.edu

This article has been accepted for publication and undergone full peer review but has not been through the copyediting, typesetting, pagination and proofreading process, which may lead to differences between this version and the Version of Record. Please cite this article as doi: 10.1002/pssr.202200497.

Introduction

Demands to support ever-increasing information traffic keep challenging the capabilities of wireless communication systems. Efficient hardware realizations of antenna devices, tailored per application, play an important role in this endeavor. While beamforming and beam steering capabilities are the cornerstone of modern 5G protocols, compact high-gain antennas are enablers for long-range point-to-point communications. There are quite a few directive antenna architectures, including those based on (i) interference phenomena between several resonant elements (e.g., Yagi-Uda), (ii) reflectors (e.g., parabolic dish), (iii) phased arrays, and several others have been demonstrated [1]. While each of those realizations has advantages in specific applications, phased arrays provide high design flexibility. In conventional phased arrays, the response of a structure is governed by an array factor. In the transmit mode, electromagnetic radiation of multiple elements is summed up coherently, forming a beam. In this case, the spatial arrangement of radiators and their relative phase shifts play a key role, especially if the number of elements is large. Owing to a high level of design flexibility and scalability, phased arrays can be made conformal to a structure [2], implemented on flexible substrates [3, 4], embedded into enclosures [5], integrated within peripheral electronic circuitry [6], and have many other engineering advances. In classical phased arrays, the inter-spacing between elements is kept wavelength-comparable, as overpopulating the area with radiators does not provide a significant advantage and comes with elevating design complexity and implementation costs. Coupling between adjacent elements within an array is also subject to reduction and is frequently neglected in early design stages.

Metamaterials [7–10], capable of controlling the propagation of electromagnetic waves almost on demand, opened a range of new frontiers in beam shaping and control. Carefully designed surfaces (metasurfaces) can tailor the properties of transmitted and reflected waves [7, 11–13]. In contrast to phased arrays, metasurfaces utilize near-field coupling between elements. Many realizations of dynamically reconfigurable metasurfaces and metasurface-based antennas have been demonstrated (e.g., [12, 14–18]). For example, tunable capacitance elements allow shifting resonant responses of individual elements, and as a result, either amplitude or phase switchable screens are achieved [12, 19, 20].

Fast-developing concepts of 5G communication protocols challenge hardware peripherals and motivate the development of new devices [21]. For example, reconfigurable antennas, aimed to

maximize data rates, spectral efficiencies, and other parameters, can be affordable by smart devices with computational capabilities (e.g., smartphones). However, other participants connected to the network can have a variety of different characteristics. For example, low-cost Internet of Things (IoT) devices can compromise performance for cost. As a result, many different architectures have been developed to match a specific application [22, 23].

In most cases, phased arrays and metasurfaces rely on two-dimensional architectures, while the third volumetric degree of freedom is unexplored. One of the main reasons here is primarily technological, as fabrication routines are based on lithography and etching. However, advances in additive manufacturing, especially 3D printing, open new opportunities in antenna design. Computer numerical control (CNC) milling [24, 25], laser direct structuring [26-28], conformal printing of metallic inks [29, 30], ultrasonic wire mesh embedding [31], stereolithography (SLA) of dielectric antennas [32, 33], and metal deposition through a mask on curved surfaces [34, 35] are among the demonstrated additive manufacturing methods aimed at providing high-quality RF components [36].

Here we propose a compact directive antenna, whose design encompasses approaches of classical phased arrays and multipole engineering to obtain directive emission with a single volumetric element. The design is based on genetic optimization, constraining several factors simultaneously on pathways to demonstrate a highly directive device with a relatively small aperture.

The manuscript is organized as follows: antenna design and optimization are discussed first and then followed by its fabrication based on 3D-printing and plastic metallization. The fabricated device is characterized and assessed versus competitive approaches. A detailed analysis of the results, including multipole decomposition of radiation patterns, is performed before the Conclusion.

Antenna design

Problem statement

The objective of our design is to obtain a high-gain antenna with a small size aperture. In the case of a non-resonant aperture with area A, the gain is limited by $G = 4\pi A/\lambda^2$, where λ is an operational wavelength. To increase the gain at the predefined frequency band, either aperture size should be increased or resonant phenomena to be employed. Theoretically, superdirective antennas can provide a high gain by utilizing multiple constructively interfering resonances accommodated within a small volume structure. However, practical restrictions, including material losses and very low tolerance to fabrication imperfections, significantly limit performances [37]. Chu-Harrington, Geyi, and other criteria have been developed to provide tighter bound [38, 39]. Several designs succeeded to overcome the previously mentioned estimates by several dBs, e.g., [40] exploiting the concept of

resonance cascading [41]. To design our device, we adopt concepts of multi-resonant elements and phased arrays to benefit from the advantages of both approaches, reducing their probable penalties.

We chose a low-GHz frequency band, as it is relevant to modern wireless communications on the one hand and demands a certain level of miniaturization on another. The starting point for the optimization was a small array of monopoles above a finite-size metal ground plane. This layout has several advantages. First, metallic reflectors can significantly improve antenna gain capabilities. Second, the ground plane allows separating a feeding network and radiating elements, preventing undesired electromagnetic coupling. To demonstrate the concept without overcomplicating the device, a four-element phased array will be investigated. This allows considering only one-quarter of the device, applying symmetric boundary conditions in the simulation. The optimization steps are summarized in Fig. 1 and are separated into two stages. The first one is optimizing the topology of the wire by discretizing it into several sections, which are allowed to move independently through maintaining electrical contact between the sections. While this approach allows obtaining completely unpredictable shapes granting superior performances, it is rather computationally expensive. Hence, we will use it for an initial crude estimate followed by the second optimization step, based on particle swarm optimization, as it will be elaborated hereinafter. The main parameters used in the algorithms are summarized in Table 1.

Genetic algorithm

In general, a genetic algorithm is a sequence of commands similar to evolutionary natural selection: heredity, mutations, and chromosomal crossover. The first task is formulating an objective function, a set of parameters undergoing optimization and constraints. Here, the initial population (the number of objects under consideration with an individual genotype) was set to encompass 64 samples. In our case, the "survival" function or the objective function is the realized gain, broadside. The antenna elements were enforced to obtain a mutually coherent feed. The algorithm is provided by the CST Studio Suite software package, where it is interfaced with electrodynamic modeling. Fast convergence of a forward solver enables performing multiple optimization steps and approaching an optimal solution, though, in this type of optimization, converging to a global extremum is not guaranteed [42]. In the first step, a curved wire was discretized into five sections to reduce the dimension of the optimization space. Each section is represented by a spherical node (Fig. 1(a)). The structure is placed on top of a flat disc, which serves as a ground plane and bounds the structure. The feeding network will be placed underneath and, consequently, can be taken out from the radiating element optimization. The genotype consists of 15 spatial coordinates for five nodes and one spatial variable for the feed - 16 numbers in total. The frequency domain solver (finite element method) was

used. The runtime on an arbitrarily selected sample did not exceed 1 minute. The result of the above optimization is quite remarkable – at the best gain (about 10 dB) the nodes were found to belong to a 3D elliptical curve. This empirical result reduces the size of the genotype quite significantly without a need to change the formulation of the problem and, as a result, significantly reduces the computational effort. Furthermore, this next step allows introducing technological limitations of further fabrication routine more precisely.

Particle swarm algorithm

The second optimization stage considers parametrized elliptical forms and their relative orientations with respect to the ground plane (Fig. 1 (b)). Notably, the first step is not mandatory, if we had preliminary knowledge that elliptical curves grant next-to-optimal performances. The following variables were used for the settled genotype: (i) lengths of semi-axis a and b, (ii) cutout angle δ, (iii) two Euler's angles φ and θ, and (iv) the distance from the origin r_0. In overall, a 6-dimensional space was chosen. To optimize this geometry, the particle swarm algorithm was chosen among others, as it is known to have a higher convergence rate in cases where an initial guess is already close to the minimum [43]. The particle swarm optimization is different from the genetic algorithm. Here, samples do not have random genotype mutations and gene crossing. However, a new generation is likely to have characteristics close to those recognized as the best at the beginning of the "extinction round". As a result, the swarm population may be smaller than in the case of a genetic algorithm, and hence the swarm is better converging to a global minimum. The settings of the particle swarm algorithm are: (i) swarm size 10, (ii) the maximal number of iterations 50, and (iii) initial distribution according to Latin hypercube distribution. Furthermore, a thin perfect electric conductor (PEC) wire model was employed to reduce the computation complexity. Finally, an integral solver, which does not require meshing a free space, was used, reducing the run time per single configuration to 30 seconds on a standard office PC (i5-8400, 2.8 GHz, RAM 16 GB). The following parameters were fixed: central frequency $f_0 = 3GHz$, the aperture size of the ground plane disk $R_0 \approx 2\lambda_0$. The optimal set of parameters appears in the inset (c) to Fig. 1.

Table 1. Summary of the main settings of the optimization algorithms.

Parameter	Setting	Description
Population size	Genetic: 64 Swarm: 10	A number of possible random sets of genes.
Max. number of iterations	Genetic: 100 Swarm: 50	A number of generations of samples.

Survival function	$0{,}5 \cdot (\text{Volumetric angle} < 2\ deg.) + 2 \cdot (\text{Realized gain} \rightarrow max.)$	Probability of survival of a sample in each generation. Here, a random initial distribution was used.
Geometry	Genetic: $(x, y, z)_i$ for i=1..5 , r_0 Swarm: 2 ellipse semi-axis, cut-out, 2 Euler angles, r_0	Parameters undergoing optimization. The algorithm chooses configurations for a new round of "extinction".

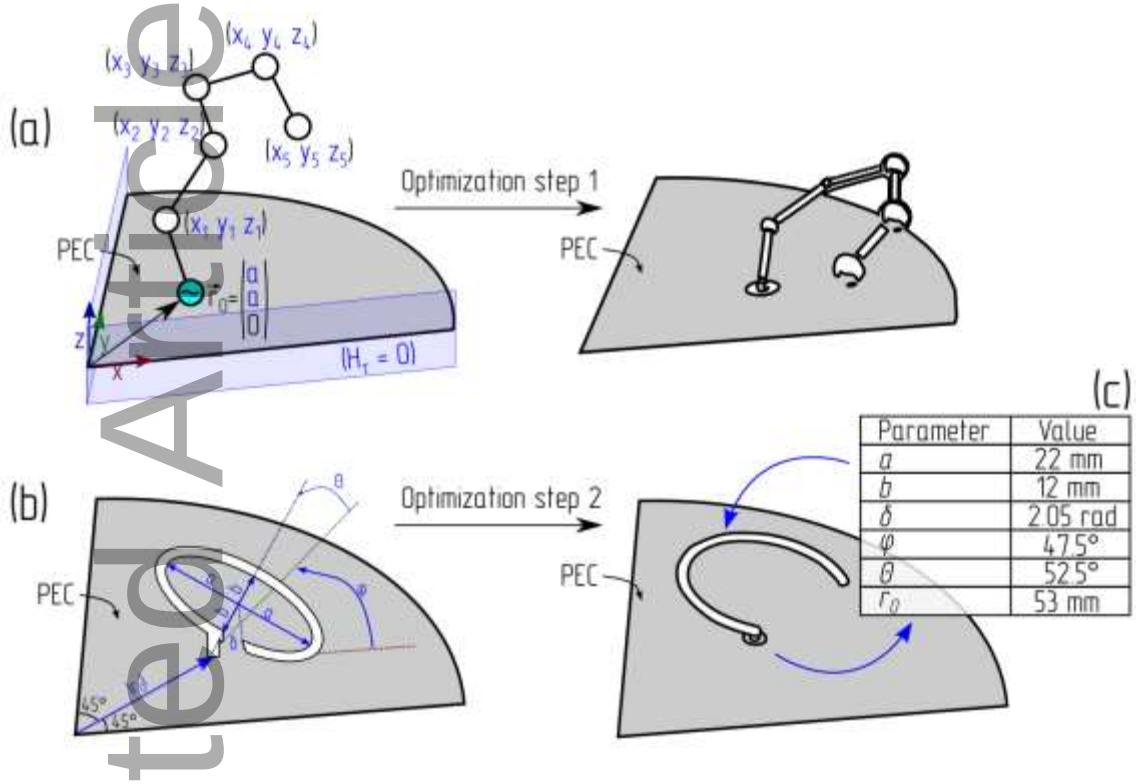

Figure 1. Two-step optimization. (a) A primary optimization by a genetic algorithm. The structure is discretized into five nodes, leading to a 16-dimensional search space. (b) The second optimization step is based on the particle swarm algorithm. The optimization is performed on an elliptic curve, resulting in a 5-dimensional search space. Inset (c) – optimal antenna parameters.

Antenna fabrication

Additive manufacturing

After obtaining the design, antenna elements are to be fabricated. While the current layout can be implemented by a manual shaping of metal wires, we exploited additive manufacturing techniques, which certainly have advantages in cases where complex 3D-shaped structures are involved. Recently, we masted several selective plastic and polymer metallization techniques [7,9–13], and an improved variation of one of those will be used hereinafter. A thiocarbamide gloss-forming agent was added to the electroplating routine. A 3D photopolymer printer Anycubic Photon Mono X was used to provide 10-micron scale fabrication accuracy. Skeletons of the radiating elements were printed first. The photopolymer resin is cured using ultraviolet lamps through the transparent bottom

of the bath and settles on the printing table. As the structures have a complex volumetric form factor, support elements are required to prevent mechanical collapse during the process. Those are manually removed by the end of the printing. The resulting elements are subsequently coated with an electrically conductive varnish and covered with in-lab-produced graphite dust with a grain size of about 50 microns. At the next stage, the skeletons were placed in a galvanic solution (300 g of copper sulfate, 200 g of sulfuric acid, 0.1 g of thiocarbamide, and 0.1 g of salt per 1 liter of solution) for 1 hour. As a result, the components were uniformly covered with copper (with surface tolerance less than 0.1 mm (see Fig. 2 (c, d)) and 0.25 mm thickness, which prevails the skin depth in the GHz range).

Power distribution

Since the Wilkinson power divider [44] is a very convenient, easy-to-implement, and widely used method for dividing a coherent signal, and maintaining the phase, in this work, we used it for matching the supply point with the array elements (Fig. 2 (b)). The final design was implemented as microstrips on the back of the reflector. The wave resistance of the microstrip line, in this case, depends mainly on its width, simplifying the optimization.

The resulting antenna is shown in Fig. 2 (a). As the radiating elements are completely sealed with the metal, their interiors play no role in electromagnetic interactions and can be ignored.

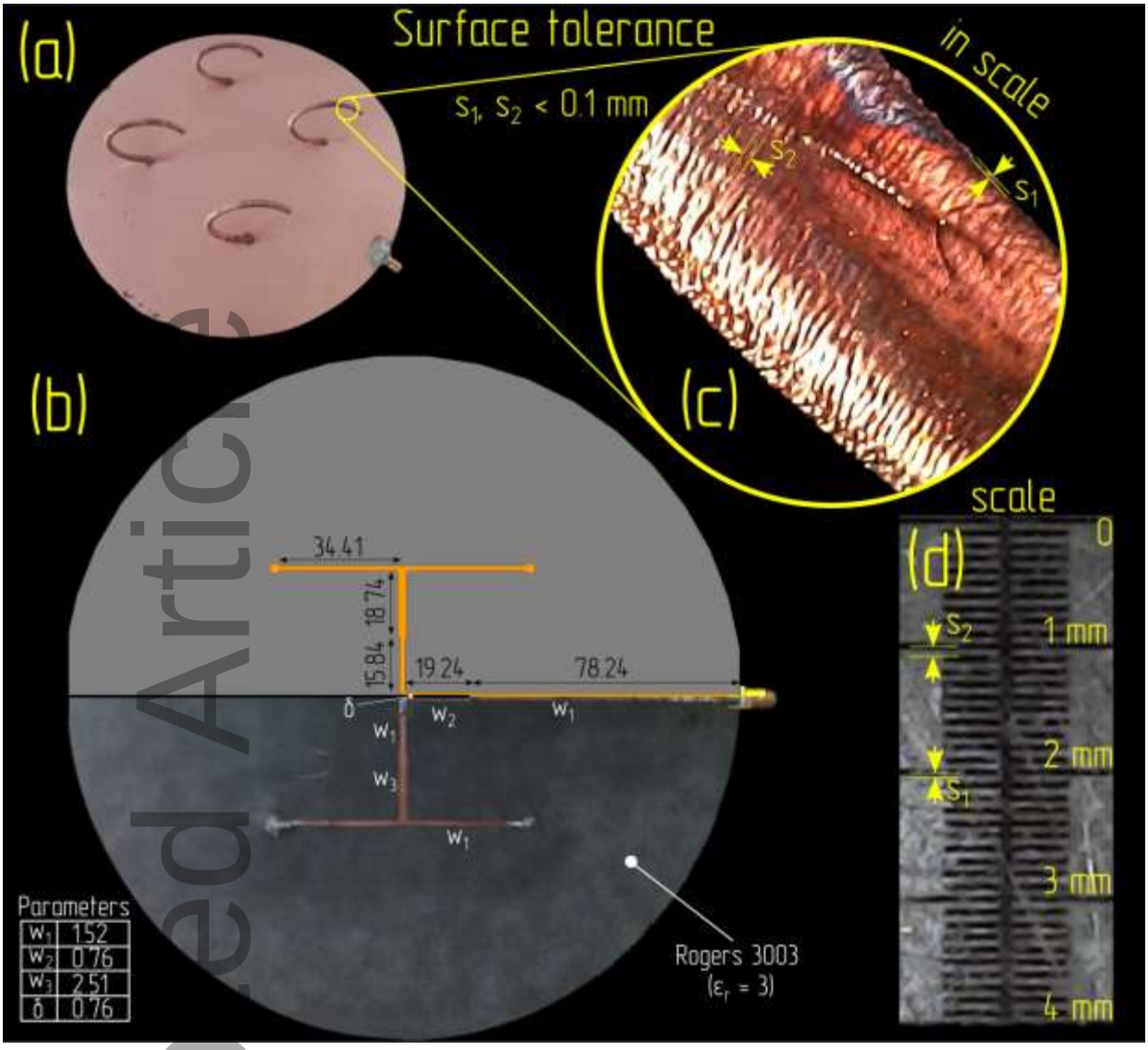

Figure 2. (a) Photograph of the fabricated antenna array. (b) Double Wilkinson power divider to feed all the elements in-phase, all values are in millimeters. (c) Zoomed image of the antenna surface with roughness estimation in scale with dashed scale (d).

Antenna Characterization

Antenna performance will be characterized next and assessed versus full-wave numerical analysis, considering all the geometrical features of the device. Four radiating elements, fabricated according to the design, are placed on a circular ground plane (R = 100 mm) and connected to feed elements. The setup for far-field measurements includes a vector network analyzer Keysight P9374A, an axial rotation mechanism with a resolution of 0.1°, and a Vivaldi antenna as a receiver. Figure 3 summarizes the results. Fig. 3 (a) is the numerically obtained realized gain spectrum (radiation efficiency follows this graph and varies between -0.2 and -0.4dB, corresponding to 4-8% energy loss). Recall that this parameter does not consider an impedance mismatch between the antenna and the feeding cable, which can be mitigated by introducing an additional and optionally tunable matching circuit. Fig. 3 (b) demonstrates numerical and experimental S_{11} parameters. Quite a remarkable

matching at the frequency where the antenna was optimized can be observed. The realized gain at the matching frequency is 14.3 dBi. Fig. 3(c) is the measured heatmap of the radiation pattern. Each vertical slice along the graph is the unwrapped realized gain pattern (linear scale) at ZX cut plane (Fig. 1). Fig. 3 (d, and e) demonstrate polar plots of the realized gain patterns, both numerical predictions and experimental data. It is noticeable that the beam at the frequencies of interest is indeed highly directional.

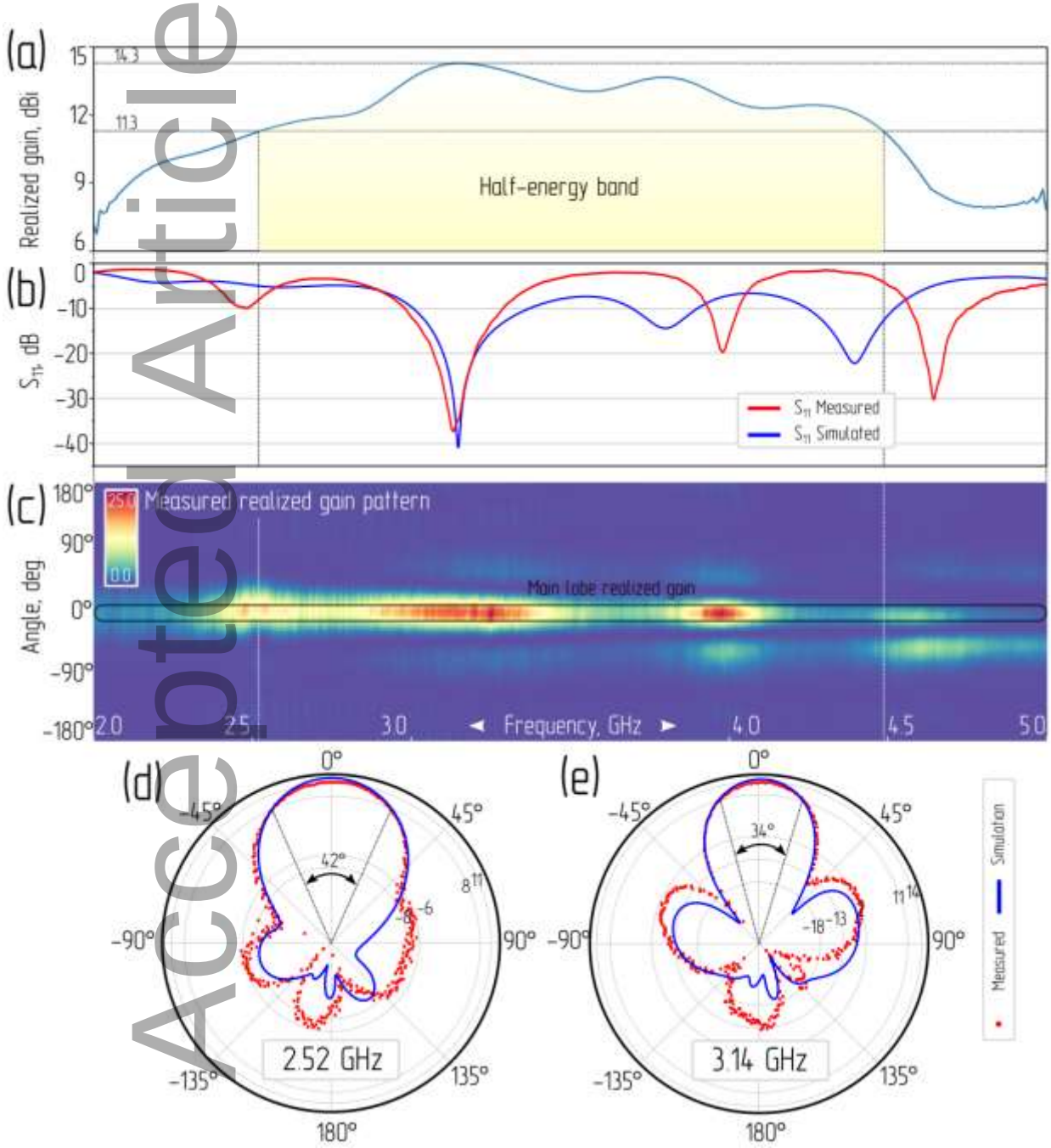

Figure 3. Phased array performance. (a) Realized gain as a function of frequency, numerical data. The frequency range, where the realized gain is greater than half the maximum, is highlighted. (b) S_{11}-parameters - numerical and experimental data. (c) Colormap, representing the radiation patterns, experimental data. Each vertical cut demonstrates the radiation pattern in ZX antenna plane. (d, e) Antenna patterns (ZX plane, Fig. 1) – numerical and experimental data.

Performance Assessment

The demonstrated antenna provides a relatively high gain (compared to the designs below) with a rather small aperture, suggesting that resonant phenomena play a role. Specifically, 14.3 dBi realized gain with 2 wavelengths diameter circular aperture has been demonstrated. This performance can be assessed versus a theoretical nonresonant limit, which can be hypothetically approached with a parabolic reflector with 100% efficiency, which provides:

$$G_{max} = 20\ \log_{10}\frac{\pi D}{\lambda} \quad (1),$$

where D is the dish diameter, and λ is the wavelength. Substituting the parameters of our phased array to Eq. 1, 16 dBi is obtained, outperforming the demonstrated antenna by only 1.7 dBi. It is worth noting that typical parabolic dish antennas have efficiencies of about 50-60%. Taking this empirical factor into account, Eq. 1 will provide a gain of around 13 dBi. Furthermore, the performances of a small aperture hypothetical dish will be further degraded owing to a power overflow at the reflector's boundaries. A detailed comparison between our realization and parabolic reflectors is presented in Table 2.

Table 2. Comparison of the antenna array with the parabolic antenna

Parameter	Parabolic antenna			Phased array [45]	Phased array [46]	This work
	Ideal	50% efficient	2λ aperture			
Aperture, mm	-		100	100 x 80	70 x 70	R = 100
Gain, dBi	16	13	< 13	13.2	< 11.25	14.3 (>11.3)
Number of elements	1			4	4	4
Frequency, GHz	3.14			3.8	3.0 - 5.0	3.14 (2.5-4.5)

We will further compare our phased array with recent reports, e.g., [45, 46], as those have both aperture dimensions and characteristic frequencies close to ours (see Table 2). In [45], a patch antenna array is demonstrated for airborne applications, while [46] concentrates on elements isolation for 5G MIMO. Our realization has the highest gain among the considered devices.

Since the output of a genetic optimization algorithm is rather unpredictable and might not follow conventional design rules, it is worth understanding the operation principles of the end product. A

detailed analysis will be performed next. As the array consists of 4 elements, it is first worth assessing their mutual isolation. The distance between the elements within the array is wavelength-comparable (from 0.625λ for nearest neighbors at 2.5 GHz to 1.6λ across diagonal at 4.5 GHz), the elements themselves (the 3D elliptical curves) are not point-like, and the ground plane has finite dimensions – all those make the isolation problem untrivial. To assess the isolation quality, mutual transmission properties were calculated numerically ($|S_{ij}|$ parameters). For this purpose, one of the antennas within the array was connected to an active port, while the other was set to operate at the receive mode. Figure 4 shows the spectra for all possible cross-scenarios. In all the cases, the isolation is better than ~25dB, confirming that the elements are visually uncoupled. In this case, the gain characteristics of the antenna are given through the antenna array factor and the properties of individual radiating elements. Furthermore, this extremely good isolation suggests the capability to extend the array size significantly and, as a result, elevate the gain.

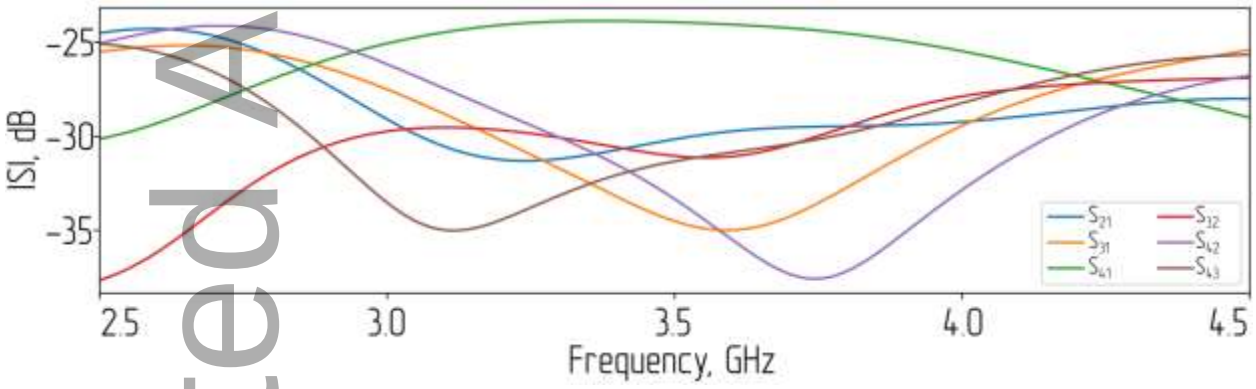

Figure 4. Numerical assessment of isolation between the array elements.

Beam steering estimations

While the radiation pattern of the demonstrated antenna is static, beam steering capabilities can be obtained by introducing phase-shifting elements into the feeding network. To assess potential performances, a numerical analysis will be done next. The optimal scheme to control a pattern of a 2x2 antenna array is to phase a pair of adjacent (nearest neighbors) elements in respect to the second pair. $\delta\varphi \in (-\pi, \pi]$ is the relative phase shift. The main lobe inclination angle α is estimated with: $\delta\varphi = \frac{2\pi}{\lambda} d \sin\alpha$, where d is for the distance between the emitters, $d = r_0\sqrt{2}$, and λ is the operating wavelength. Then maximal inclination α_{max} is obtained for $\delta\varphi = \pi$, leading to $(d \sim \lambda)$ $\alpha_{max} \approx 30°$. However, due to the small number of elements in the antenna array, a significant part of the energy will also go to the first diffraction maximum, creating the side lobe.

Figure 5 summarizes the beam steering capabilities and assesses the contribution of the secondary side lobe. A two-dimensional grid allows performing scanning in two orthogonal planes, ZX and YZ, as indicated in Fig. 1 (a).

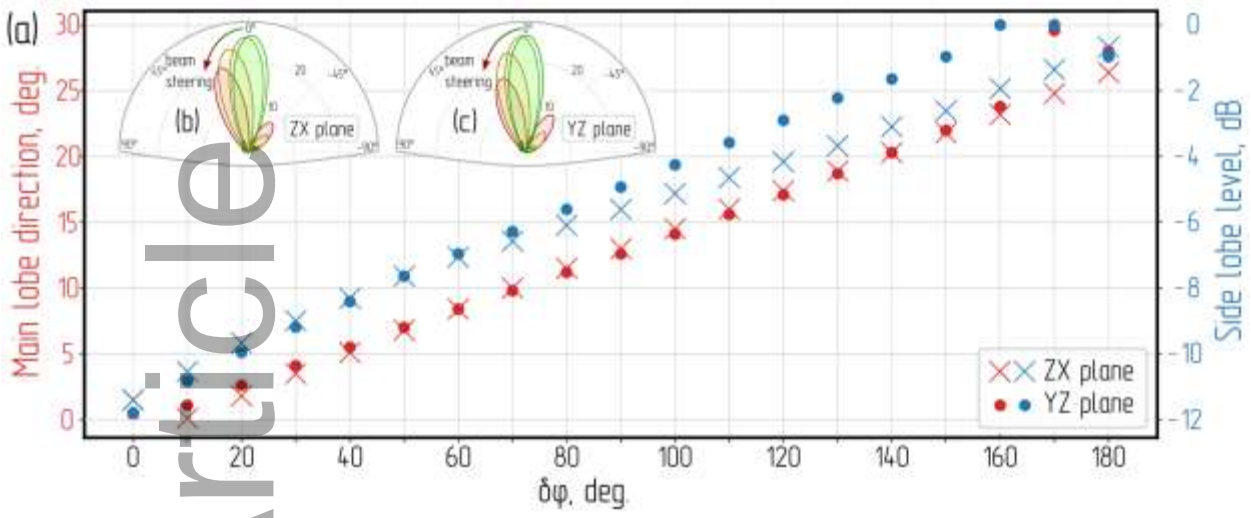

Figure 5. Beam steering capabilities, numerical results for 3.14 GHz. (a) Red, left axis – main lobe direction. Blue, right axis – side lobe level, as a function of the relative phase between the pairs of the elements. (b), (c) – radiation patterns at ZX and YZ planes, respectively.

Multipole expansion

The last step is to investigate the radiation properties of the array for revealing the presence of an additional resonant phenomenon, granted by genetic optimization. Since our realization consists of 4 genetically designed radiators above a ground plane, it is appealing to compare it with a relevant, frequently used architecture of a helical antenna array. The schematic representations of the antennas, subject to further comparison, appear in Fig. 6. Figure 6 (a) shows the proposed design, while Fig. 6 (d) shows a model of an array of four helical antennas. The ground plane reflector in both cases is kept the same. The helical array has a similar gain of 13.3 dBi at 3.75 GHz. The pronounced difference is the much larger volume occupied by the helical antenna. Furthermore, the spiral antenna radiates a circular polarization [47], while our design has an elliptical one (close to linear).

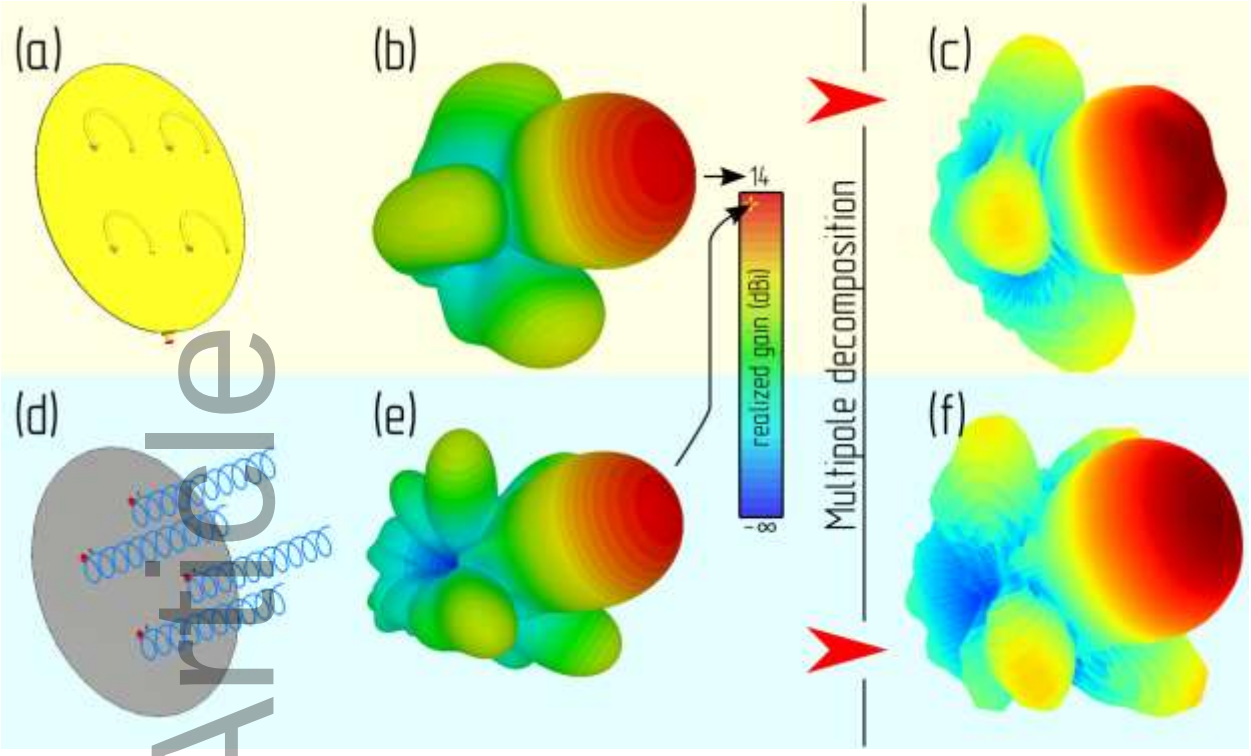

Figure 6. Comparison between the antennas. Layouts - (a) and (d). Far-field radiation patterns, numerical results- (b) and (e). Radiation patterns reconstructed from the multipole expansion - (c) and (f).

Multipole expansion will be applied to demonstrate the resonant nature of the device, which grants it an extra-directivity (e.g., better than a dipole). The expansion is performed based on spherical harmonics, forming a complete set of functions on a sphere [48].

$$Y_l^m(\theta,\varphi) = (-1)^m \sqrt{\frac{(2l+1)!}{4\pi}\frac{(l-m)!}{(l+m)!}} P_l^m(\cos\theta) e^{im\varphi} \text{ for } l = \overline{0,1,\ldots}, m = \overline{-l,\ldots,0,\ldots,+l} \quad (2),$$

where $P_l^m(\cos\theta)$ is for the associated Legendre polynome, and the standard spherical coordinate system is considered.

The expansion results appear in Fig. 7, where both amplitudes and phases are calculated. The multipole spectra of the antennas are different. While the coefficients $a_{l,-1}$ dominate for the helical geometry (as a consequence, such an antenna is circularly polarized), the components $a_{l<10,m=\pm1}$ ($a_{l>11,m=\pm3}$) are dominant in the geometry we propose. Consequently, elliptical polarization and high gain with a small volume are obtained. Considering the multipole series, it can be noticed that the helical antenna converges quite quickly, while much more coefficients must be taken into account for our generic antenna. It is noticeable that while the helical antenna is represented by the only one -/*m*/-component of the multipole decomposition for each *l*, the proposed sample has a symmetrical +/*m*/-component that causes the proximity of its polarization to linear one. Hence, the coherent superposition of numerous higher-order multipoles, engineered with the aid of the genetic

optimization, is the key underlining concept that allows to obtain an elevated gain in a relatively small footprint device.

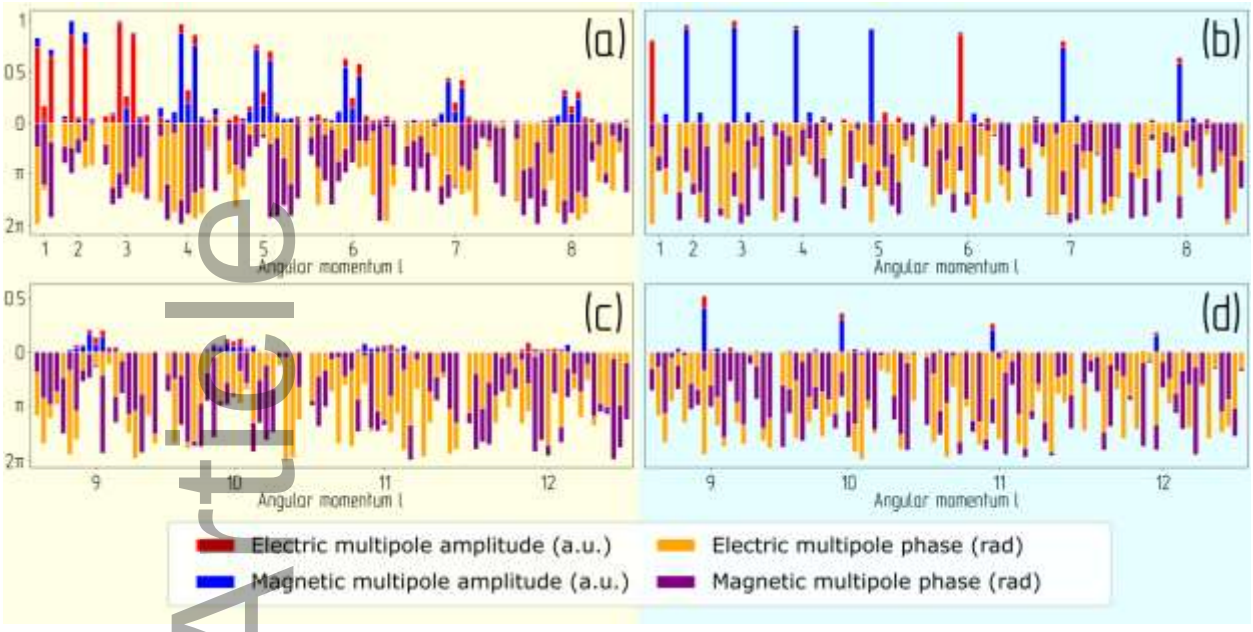

Figure 7. Multipole expansion of radiation patterns - up to 12th order for the proposed geometry – (a), (c), for helical antenna – (b), (d).

Conclusion

Recent advances in additive manufacturing and accurate surface metallization of plastic elements motivate considering complex volumetric antenna architectures on pathways to obtain superior performances. Here we demonstrated a 4-element phased array, designed with fast 2-step optimization, encompassing genetic and swarm optimization stages. The detailed analysis of the outcome indicated that all the elements appear to be decoupled, demonstrating better than 25dB isolation within the array. Furthermore, each radiating element and, as a result, the array as a whole, encompass a large number of resonating multipoles, coherently contributing to a directive beam formation. The concept was realized and demonstrated 11-12dB gain with an aperture as small as 2λ. Our design demonstrates performances comparable to those of high-grade parabolic reflectors without a penalty of high weight and cost. Furthermore, our approach can be extended to larger arrays, encompassing multiple elements. In this case, fast prototyping and manufacturing, granted by additive manufacturing techniques, can have significant advantages over conservative antenna designs.

Acknowledgments

The research was supported by the Federal Academic Leadership Program Priority 2030. The authors thank Dr. Elena Bazanova for her critical reading of the manuscript.

References

[1] C.E. Balanis, Antenna Theory: Analysis and Design, 3rd Edition - Constantine A. Balanis, A JOHN WILEY & SONS, INC, Pages: 1136, 2005

[2] H. Schippers, J. Verpoorte, P. Jorna, A. Hulzinga, A. Meijerink, C. Roeloffzen, R.G. Heideman, A. Leinse & M. Wintels, "Conformal phased array with beam forming for airborne satellite communication", 2008 International ITG Workshop on Smart Antennas, 2008, pp. 343-350

[3] M.R.M. Hashemi, A.C. Fikes, M. Gal-Katziri, B. Abiri, F. Bohn, A. Safaripour, M.D. Kelzenberg, E.L. Warmann, P. Espinet, N. Vaidya, E.E. Gdoutos, C. Leclerc, F. Royer, S. Pellegrino, H.A. Atwater, A. Hajimiri, A flexible phased array system with low areal mass density, Nature Electronics 2019 2:5. 2 (2019) 195–205

[4] M. Gal-Katziri, A. Fikes, F. Bohn, B. Abiri, M.R. Hashemi, A. Hajimiri, Scalable, deployable, flexible phased array sheets, IEEE MTT-S International Microwave Symposium Digest. 2020-August (2020) 1085–1088

[5] D. G. Kam, D. Liu, A. Natarajan, S. K. Reynolds and B. A. Floyd, "Organic Packages With Embedded Phased-Array Antennas for 60-GHz Wireless Chipsets," in IEEE Transactions on Components, Packaging and Manufacturing Technology, vol. 1, no. 11, pp. 1806-1814, Nov. 2011

[6] Q. -Q. He, S. Ding, C. Xing, J. -Q. Chen, G. -Q. Yang and B. -Z. Wang, "Research on Structurally Integrated Phased Array for Wireless Communications," in IEEE Access, vol. 8, pp. 52359-52369, 2020

[7] N. Engheta, R. Ziolkowski, Electromagnetic Metamaterials: Physics and Engineering Explorations, 2006

[8] D. Filonov, A. Shmidt, A. Boag, P. Ginzburg, Artificial localized magnon resonances in subwavelength meta-particles, Appl Phys Lett. 113 (2018) 123505

[9] V.S. Asadchy, M. Albooyeh, S.N. Tcvetkova, A. Díaz-Rubio, Y. Ra'Di, S.A. Tretyakov, Perfect control of reflection and refraction using spatially dispersive metasurfaces, Phys Rev B. 94 (2016) 075142

[10] F. Capolino, Applications of Metamaterials, Applications of Metamaterials. (2017)

[11] N.I. Zheludev, Y.S. Kivshar, From metamaterials to metadevices, Nat Mater. 11 (2012) 917–924

[12] V. Kozlov, D. Vovchuk, P. Ginzburg, Broadband radar invisibility with time-dependent metasurfaces, Scientific Reports 2021 11:1. 11 (2021) 1–11

[13] M. Faenzi, G. Minatti, D. González-Ovejero, F. Caminita, E. Martini, C. Della Giovampaola, S. Maci, Metasurface Antennas: New Models, Applications and Realizations, Scientific Reports 2019 9:1. 9 (2019) 1–14

[14] H.-X. Xu, S. Tang, S. Ma, W. Luo, T. Cai, S. Sun, Q. He, L. Zhou, Tunable microwave metasurfaces for high-performance operations: dispersion compensation and dynamical switch, Sci Rep. 6 (2016) 38255

[15] D.F. Sievenpiper, J.H. Schaffner, H.J. Song, R.Y. Loo, G. Tangonan, Two-dimensional beam steering using an electrically tunable impedance surface, IEEE Trans Antennas Propag. 51 (2003) 2713–2722

[16] W. Yang, L. Gu, W. Che, Q. Meng, Q. Xue, C. Wan, A novel steerable dual-beam metasurface antenna based on controllable feeding mechanism, IEEE Trans Antennas Propag. 67 (2019) 784–793

[17] X. Wang, S. Tretyakov, From Tunable and Reconfigurable to Space-Time Modulated Multifunctional Metasurfaces, 2021 IEEE International Symposium on Antennas and Propagation and North American Radio Science Meeting, APS/URSI 2021 - Proceedings. (2021) 1361–1362

[18] M. Di Renzo, A. Zappone, M. Debbah, M.S. Alouini, C. Yuen, J. De Rosny, S. Tretyakov, Smart Radio Environments Empowered by Reconfigurable Intelligent Surfaces: How It Works, State of Research, and the Road Ahead, IEEE Journal on Selected Areas in Communications. 38 (2020) 2450–2525

[19] D. Ramaccia, D.L. Sounas, A. Alu, A. Toscano, F. Bilotti, Phase-Induced Frequency Conversion and Doppler Effect with Time-Modulated Metasurfaces, IEEE Trans Antennas Propag. 68 (2020) 1607–1617

[20] J.J. Luther, S. Ebadi, X. Gong, A microstrip patch electronically steerable parasitic array radiator (ESPAR) antenna with reactance-tuned coupling and maintained resonance, IEEE Trans Antennas Propag. 60 (2012) 1803–1813

[21] H. Asplund, D. Astely, P. Butovitsch, T. Chapman, M. Frenne, F. Ghasemzadeh, M. Hagström, B. Hogan, G. Jongren, J. Karlsson, F. Kronestedt & E. Larsson – Advanced Antenna Systems for 5G Network Deployments: Bridging the Gap Between Theory and Practice, 1st Edition | Academic Press; 1st edition (July 6, 2020).

[22] S. Kumar, A. Dixit, R. Malekar, H. Raut, L. Shevada – Fifth Generation Antennas: A Comprehensive Review of Design and Performance Enhancement Techniques. IEEE Access (2020), 10.1109/ACCESS.2020.3020952.

[23] N. Kishore, A. Senapati – 5G smart antenna for IoT application: A review, Int J Commun Syst, Vol. 35, Issue 13, 2022, 1074-5351.

[24] Ferrando-Rocher, M., Herranz, J. I., Valero-Nogueira, A. & Bernardo, B. Performance assessment of gap waveguide array antennas: CNC milling vs. 3D printing. IEEE Antennas Wirel. Propag. Lett.

[25] Al-Tarifi, M. A. & Filipovic, D. S. On the design and fabrication of W-band stabilised-pattern dual-polarised horn antennas with DMLS and CNC. IET Microw. Antennas Propag. 11(14), 1930–1935

[26] Sonnerat, F., Pilard, R., Gianesello, F., Le Pennec, F., Person, C. & Gloria, D. Innovative LDS antenna for 4G applications. In IEEE, no. Eucap, 2696–2699 (2013).

[27] Friedrich, A., Fengler, M., Geck, B. & Manteuffel, D. 60 GHz 3D integrated waveguide fed antennas using laser direct structuring technology. In 2017 11th European Conference on Antennas and Propagation, EUCAP 2017 2507–2510 (2017)

[28] Friedrich, A. & Geck, B. On the design of a 3D LTE antenna for automotive applications based on MID technology. Eur. Microw. Conf.

[29] J. Adams, S. Slimmer, T. Malkowski, E. Duoss, J. Lewis & J. Bernhard. Comparison of spherical antennas fabricated via conformal printing: Helix, meanderline, and hybrid designs. IEEE Antennas Wirel. Propag. Lett. 10, 1425–1428

[30] Ahmadloo, M. Design and fabrication of geometrically complicated multiband microwave devices using a novel integrated 3D printing technique. In 2013 IEEE 22nd Conference on Electrical Performance of Electronic Packaging and Systems 29–32 (2013)

[31] Liang, M., Shemelya, C., MacDonald, E., Wicker, R. & Xin, H. 3-D printed microwave patch antenna via fused deposition method and ultrasonic wire mesh embedding technique. IEEE Antennas Wirel. Propag. Lett. 14, 1346–1349

[32] S. Wang; F. Fan; Y. Xu; Z. Guo; W. Zheng; Y. Liu and Y. Li, "3-D Printed Zirconia Ceramic Archimedean Spiral Antenna: Theory and Performance in Comparison With Its Metal Counterpart," in IEEE Antennas and Wireless Propagation Letters, vol. 21, no. 6, pp. 1173-1177, June 2022

[33] S. Wang, W. Ge, G. Zhang, Y. Li, S. -W. Wong and L. Zhu, "3-D Printed Metallic CP Antenna With Dual-Cavity Structure and Enhanced Axial Ratio Bandwidth," 2020 IEEE Asia-Pacific Microwave Conference (APMC), Hong Kong, Hong Kong, 2020, pp. 236-238

[34] Ehrenberg, I., Sarma, S., Steffeny, T. & Wuy, B.-I. Fabrication of an X-Band conformal antenna array on an additively manufactured substrate. In 2015 IEEE International Symposium on Antennas and Propagation & USNC/URSI National Radio Science Meeting 609–610 (2015)

[35] Wu, B. -I. & Ehrenberg, I. Ultra conformal patch antenna array on a doubly curved surface. In 2013 IEEE International Symposium on Phased Array Systems and Technology 792–798 (2013)

[36] D. Filonov, S. Kolen, A. Shmidt, Y. Shacham-Diamand, A. Boag & P. Ginzburg, (2019). Volumetric 3D-Printed Antennas, Manufactured via Selective Polymer Metallization. Physica Status Solidi - Rapid Research Letters

[37] R.C. Hansen, Electrically Small, Superdirective, and Superconducting Antennas, John Wiley & Sons, Inc., 2006.

[38] L. J. Chu , "Physical Limitations of Omni-Directional Antennas", Journal of Applied Physics 19, 1163-1175 (1948)

[39] W. Geyi, "Physical limitations of antenna," in IEEE Transactions on Antennas and Propagation, vol. 51, no. 8, pp. 2116-2123, Aug. 2003

[40] K. P. Nagarjun, Piyush Raj, Vadivukkarasi Jeyaselvan, Shankar Kumar Selvaraja, and V. R. Supradeepa, "Microwave power induced resonance shifting of silicon ring modulators for continuously tunable, bandwidth scaled frequency combs," Opt. Express 28, 13032-13042 (2020)

[41] S. Liu, K. Wu, L. Zhou, X. Xiao, Y. Zhong, and J. Chen, "Optical frequency comb generation and microwave synthesis with integrated cascaded silicon modulators," in 2018 Conference on Lasers and Electro-Optics, CLEO 2018 - Proceedings, OSA Technical Digest (Online) (Optical Society of America, 2018), p. JW2A.56.

[42] Holland, John H. "Genetic algorithms." Scientific american 267.1 (1992): 66-73.

[43] D. W. Boeringer and D. H. Werner, "Particle swarm optimization versus genetic algorithms for phased array synthesis," in IEEE Transactions on Antennas and Propagation, vol. 52, no. 3, pp. 771-779, March 2004

[44] Wilkinson, E.J. (1960). An N-Way Hybrid Power Divider. , 8(1), 0–118

[45] H. Sajjad, W.T. Sethi, K. Zeb, A. Mairaj, Microstrip patch antenna array at 3.8 GHz for WiMax and UAV applications, 2014 International Workshop on Antenna Technology: Small Antennas, Novel EM Structures and Materials, and Applications, IWAT 2014. (2014) 107–110

[46] M. Alibakhshikenari, B.S. Virdee, H. Benetatos, E.M. Ali, M. Soruri, M. Dalarsson, M. Naser-Moghadasi, C.H. See, A. Pietrenko-Dabrowska, S. Koziel, S. Szczepanski, E. Limiti, An innovative antenna array with high inter element isolation for sub-6 GHz 5G MIMO communication systems, Scientific Reports 2022 12:1. 12 (2022) 1–13

[47] Kraus, J. D. (1949). The helical antenna. Proceedings of the IRE, 37(3), 263-272.

[48] J. David, Classical Electrodynamics , 3rd Edition | Wiley Classical Electrodynamics , 3rd Edition Classical Electrodynamics , 3rd Edition | Wiley, 2021 (2021) 2–3.

This paper demonstrates a compact phased antenna array at 2.5-4.5 GHz, consisting of 4 elements, designed using optimization algorithms and manufactured using additive technologies of 3D printing and surface metallization. Due to the special 3D shape, the contributions of elementary modes add up constructively, and the final performance of this phased antenna array has a record gain.